Supporting Information

Qi et al. 10.1073/pnas.1421878112

SI Materials and Methods

Plant Material and Growth Conditions. Tomato (*Solanum lycopersicum*) cultivar Castlemart was used for all experiments unless otherwise stated. Tomato plants were grown in MS medium and grown under controlled conditions (25 °C at 60% humidity, with 16 h of light and 8 h of dark) until the fifth to seventh plastochron stage was reached. Shoot apices were dissected, leaving only P_1, or P_1 and P_2, intact together with a subapical region, and cultured on MS medium containing 1 μg/mL *t*-zeatin (PhytoTechnology Laboratories), 100 μg/mL myo-insitol (Sigma-Aldrich), and 0.5 μg/mL folic acid (Sigma-Aldrich) at 25 °C, with 16 h of light and 8 h of dark cycle (1). For live imaging, transgenic line *pAtPIN1::AtPIN1-GFP* in the cultivar Moneymaker background or *DR5::3×Venus-N7* in the cultivar M82 background was used instead (2).

Arabidopsis thaliana ecotypes Col-0, L*er*, Ws, and Enkheim were used. The *pin1-1* and *rev-1* mutants are in the Enkheim background (3), the *pin1-6* and *pid-7.2.1.6* mutants are in the Ws background (4), the *pin1-4* mutant and the *pPIN1::PIN1-GFP* line are in the L*er* background (5), and the *rev-6* mutant and *p35S::DII-Venus* and *pMP::MP-GFP* lines are in the Col-0 background (6, 7). Seeds were sown in pots or in plates with MS medium. Plants were incubated at 22 °C with 16 h of light and 8 h of dark unless otherwise stated.

Construction of Transgenic Plants. *pMP::MP*Δ contains the endogenous *MP* promoter (3,302 kb upstream of the start codon) and the endogenous *MP* transcriptional termination sequence (730 bp downstream of the stop codon). *MP*Δ encodes amino acids 1–813 of MP without extra residues (8). In *pAS2::MP*Δ, *MP*Δ is controlled by the *AS2* promoter containing 3,303 bp upstream of the *AS2* start codon and 18 bp of the N-terminal *AS2* coding region (9). These constructs were transformed into Col-0 plants, and >12 independent stable transformants were characterized for each construct.

Microsurgery. Separation of the site of incipient primordium formation and the meristem was carried out with syringe tips (BD Ultra-Fine Insulin Syringe). The sharp edge of the syringe tip was used to superficially scratch the tissue (1).

Chemical Treatments. For NPA treatment of *p35S::DII-Venus Arabidopsis* plants, 2.5 DAG seedlings grown on 1/2 MS medium were soaked in 50 μM NPA with 0.02 mM NaOH, or 0.02 mM NaOH only as control, and live imaging was performed after 5 h.

Local treatments of leaf primordial were following published protocols (10–13). Briefly, 1 M stock solutions of IAA, NAA, 2,4-D, NPA, or BFA (all from Sigma-Aldrich) in DMSO were dissolved in lanolin (Sigma-Aldrich) prewarmed at 50 °C to a final concentration of 10 mM each, except at 50 μM for BFA. The paste was manually administered to cultured tomato apices with syringe tips or tomato trichome tips as shown in Fig. S4 *A* and *B*.

Tissue Preparation for Confocal Analysis. Shoot apices with leaves removed were collected and immediately placed in 2.5% (wt/vol) paraformaldehyde (PFA; Sigma-Aldrich) at pH 7.0 at 4 °C, vacuum infiltrated for 30 min, and were stored overnight at 4 °C. Fixed tissue samples were then washed with 10% (wt/vol) sucrose and 1% PFA at pH 7.0 for 20 min, with 20% (wt/vol) sucrose and 1% PFA at pH 7.0 for 20 min, and 30% (wt/vol) sucrose and 1% PFA at pH 7.0 for 30 min. Samples were then embedded in 5–7% (wt/vol) LM agarose (Promega) liquid gel at 30 °C and placed at 4 °C for 15 min to solidify. Sections of 40 μm to 70 μm were made by using a Leica VT1000S vibrating-blade microtome. For high-resolution images, samples were stained with 50 μg/mL propidium iodide (PI; Sigma-Aldrich).

Confocal Microscopy, Optical Microscopy, and Electron Microscopy. Images were taken with a Zeiss LSM 510 Meta or a Nikon C2 Si confocal microscope. Excitation and detection windows setups for GFP, Venus, DsRed, Alexa Fluor 488, and Alexa Fluor 555 were as described (5, 14). To detect the signal of PI staining, a 488-nm laser line was used for excitation and a 585- to 615-nm band-pass filter was used for detection. Autofluorescence was excited at 488 nm and detected in the 660- to 700-nm range.

Leaves were fixed in fresh FAA solution under vacuum for 15–20 min, dehydrated in an ethanol series to 100%, and embedded in Paraplast Plus (Leica) or HistoResin mounting media (Leica). Sections were cut at 8 μm or 2 μm with Leica rotary microtomes, mounted on slides, and stained with 0.1% toluidine blue. Photographs were taken with a Nikon SMZ1000 stereoscopic microscope or an Olympus BX60 microscope equipped with a Nikon DS-Ri1 camera head. Scanning electron microscopy was performed by using a Hitachi S-3000N variable pressure scanning electron microscope after standard tissue preparation as described (14).

Image Processing for Polarity Visualization. Selected meristem regions were acquired with high spatial resolution (60× objective, N.A. = 1.0) and processed to clearly reveal polarization of PIN1. The PI (red) and AtPIN1-GFP (green) channels of confocal slices were processed separately but each subject to exactly the same processing steps. These steps consisted of image filtering to reduce noise and improve contrast followed by mathematical morphology operations to sharpen the location of PIN1 with respect to PI. The noise in each slice of a confocal stack was gradually reduced by using four iterations of the nonlocal means filter (15). We compared similarities of 9×9 patches in 15×15 neighborhoods around each pixel and set $h = 1.5$ as the filtering parameter. We kept these same parameters in all four iterations. Denoising helped concentrate the signals of PIN1 and PI on ridgelines without shifting their true location—a typical advantage of the nonlocal means filter. To compensate the reduction of contrast caused by denoising, we boosted back the signal by using a strong unsharp mask filter. To have the ridgelines well defined, we then eroded this sharpened image with a disk of radius two. After this step, the relative location of PIN1 with respect to PI is clearly visible (Figs. S10 and S11).

Because PI and PIN1 coexist almost at the same location, we were extra cautious during image acquisition to prevent accidently shifting their signals, which would result in the wrong polarization interpretation. To verify whether the signals we were collecting were suffering from relative shifting of green and red channels due to microscope alignment, chromatic aberration, sample movement during scanning, or other causes, we calibrated our microscope, checked signal intensity profiles, and imaged Invitrogen Tetraspeck beads in both channels. All indicated there was no signal shifting. As a final test, we imaged meristem samples at their regular position and then at 180° rotation. The cell wall and PIN1 signals were consistently found in the same relative positions and separated by the same distance, indicating that they were persistent and not shifting with either unidirectional or bidirectional scanning.

Accession Numbers. Accession numbers are the following: *AS2* (At1g65620), *MP* (At1g19850), *PID* (At2g34650), *PIN1* (At1g73590), and *REV* (At5g60690).

1. Reinhardt D, Frenz M, Mandel T, Kuhlemeier C (2005) Microsurgical and laser ablation analysis of leaf positioning and dorsoventral patterning in tomato. *Development* 132(1):15–26.
2. Bayer EM, et al. (2009) Integration of transport-based models for phyllotaxis and midvein formation. *Genes Dev* 23(3):373–384.
3. Okada K, Ueda J, Komaki MK, Bell CJ, Shimura Y (1991) Requirement of the auxin polar transport system in early stages of *Arabidopsis* floral bud formation. *Plant Cell* 3(7):677–684.
4. Furutani M, et al. (2004) *PIN-FORMED1* and *PINOID* regulate boundary formation and cotyledon development in *Arabidopsis* embryogenesis. *Development* 131(20): 5021–5030.
5. Heisler MG, et al. (2005) Patterns of auxin transport and gene expression during primordium development revealed by live imaging of the *Arabidopsis* inflorescence meristem. *Curr Biol* 15(21):1899–1911.
6. Vernoux T, et al. (2011) The auxin signalling network translates dynamic input into robust patterning at the shoot apex. *Mol Syst Biol* 7:508.
7. Schlereth A, et al. (2010) MONOPTEROS controls embryonic root initiation by regulating a mobile transcription factor. *Nature* 464(7290):913–916.
8. Krogan NT, Berleth T (2012) A dominant mutation reveals asymmetry in *MPIARF5* function along the adaxial-abaxial axis of shoot lateral organs. *Plant Signal Behav* 7(8):940–943.
9. Iwakawa H, et al. (2007) Expression of the *ASYMMETRIC LEAVES2* gene in the adaxial domain of *Arabidopsis* leaves represses cell proliferation in this domain and is critical for the development of properly expanded leaves. *Plant J* 51(2):173–184.
10. Wang Q, Kohlen W, Rossmann S, Vernoux T, Theres K (2014) Auxin depletion from the leaf axil conditions competence for axillary meristem formation in *Arabidopsis* and tomato. *Plant Cell* 26(5):2068–2079.
11. Reinhardt D, et al. (2003) Regulation of phyllotaxis by polar auxin transport. *Nature* 426(6964):255–260.
12. Stieger PA, Reinhardt D, Kuhlemeier C (2002) The auxin influx carrier is essential for correct leaf positioning. *Plant J* 32(4):509–517.
13. Reinhardt D, Mandel T, Kuhlemeier C (2000) Auxin regulates the initiation and radial position of plant lateral organs. *Plant Cell* 12(4):507–518.
14. Wang Y, et al. (2014) The stem cell niche in leaf axils is established by auxin and cytokinin in *Arabidopsis*. *Plant Cell* 26(5):2055–2067.
15. Cunha A, et al. (2012) Computational analysis of live cell images of the *Arabidopsis thaliana* plant. *Methods Cell Biol* 110:285–323.

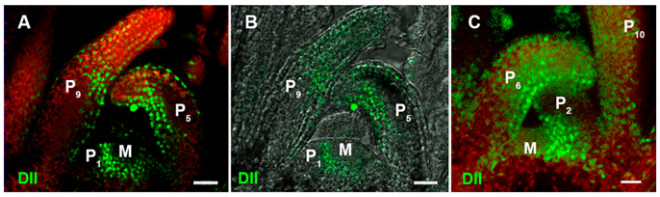

Fig. S1. Expression of DII-VENUS (green) in the vegetative shoot apex and leaf primordia. (*A*–*C*) Longitudinal section of *Arabidopsis* vegetative shoot apexes expressing DII-Venus (green) and chlorophyll autofluorescence (red). (*B*) View of the same shoot apex section as in *A* with maximum intensity projections of Nomarski interference contrast images overlaid with single optical sections of Venus. Stronger DII-Venus signals in the boundary and adjacent adaxial domain indicated weaker auxin signaling input. (Scale bars: 20 μm.)

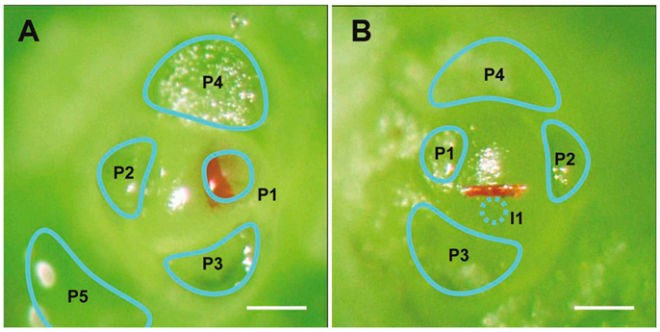

Fig. S2. Control microapplication treatment of tomato apices. (*A*) Lanolin paste (red) at the adaxial domain of an emerging primordium (P_1). (*B*) Lanolin line (red) between an incipient primordium (I_1) and the meristem. (Scale bars: 100 μm.)

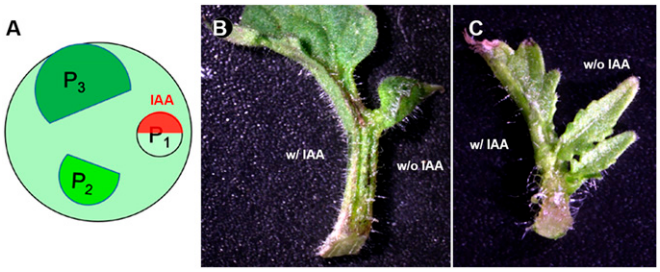

Fig. S3. Local microapplication to half of an emerging P_1 primordium leads to conversion to simple leaf form in the treated region. (*A*) Cartoon showing local IAA microapplication. (*B* and *C*) Tomato leaves after IAA microapplication shown in *A*.

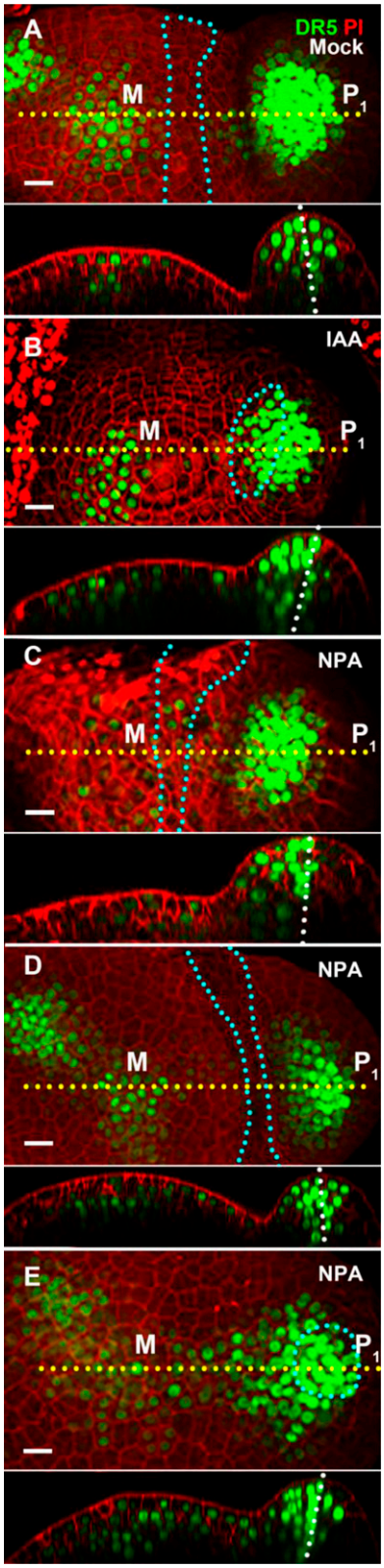

Fig. S4. Effects of IAA and NPA on auxin signaling. Upper image of each panel shows maximum intensity projections of tomato *pDR5::3XVenus-N7* expressing-meristems view from above, whereas lower images represent longitudinal sections along the planes of sections depicted by yellow dotted lines in upper images. Tomato meristems were treated with lanolin paste alone (*A*), with IAA-containing lanolin paste on the adaxial domain (*B*), or with NPA-containing lanolin paste outside the primordium (*C*), along the boundary (*D*), or at the primordium tip (*E*), with treated area highlighted by blue circles. Images were acquired 12 h (*B*) or 24 h (*A* and *C*–*E*) after treatment. The white dotted line in lower images represents the adaxial-abaxial midline. Note the Venus signal shift to the adaxial side in *B* and *C*, compared with *A*. The slight difference in auxin signaling in tomato and DII-Venus reported auxin concentration in *Arabidopsis* is likely a consequence of domain-specific expression of downstream transcription factors (Fig. 2), or incomplete reflection of auxin signaling by the *DR5* promoter (D. Weijers, personal communication). (Scale bars: 20 μm.)

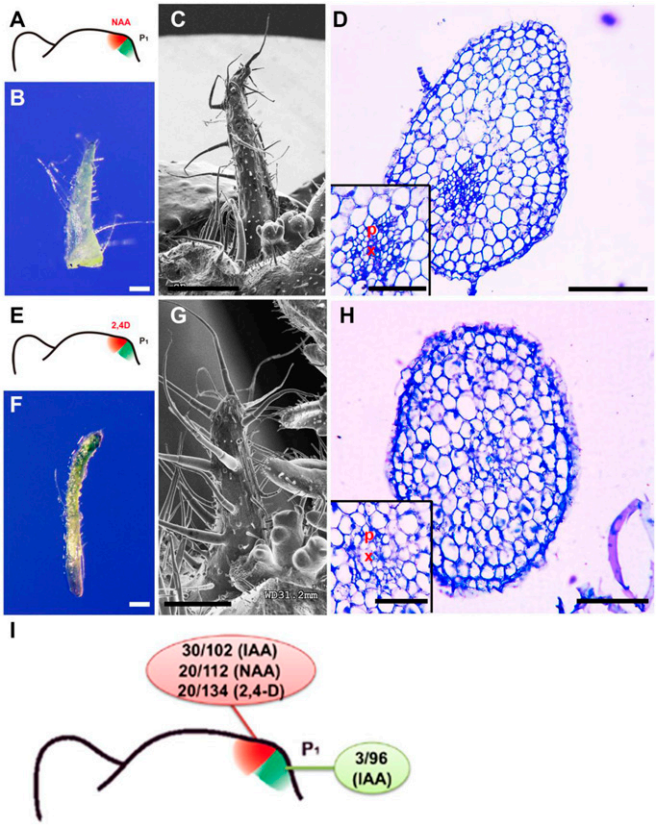

Fig. S5. Microapplication of auxin analogs induces abaxialized radially symmetric leaf primordia. (*A–D*) Tomato leaf primordia after local NAA microapplication (*A*), showing early leaf (*B*) and more mature (*C*) primordia with strong defects in adaxial-abaxial polarity, and a transverse section through the midrib and adjacent laminal regions (*D*). (*E–H*) Tomato leaf primordia after local 2,4-D microapplication (*E*), showing early leaf (*F*) and more mature (*G*) primordia with strong defects in adaxial-abaxial polarity, and a transverse section through the midrib and adjacent laminal regions (*H*). (*I*) Summary of microapplication auxin or auxin analogs on leaf polarity. IAA, NAA, or 2,4-D treatment at the adaxial domain leads to high ratios of polarity defects, whereas IAA treatment at the abaxial domain leads to a low ratio of polarity defects. (Scale bars: 20 μm.)

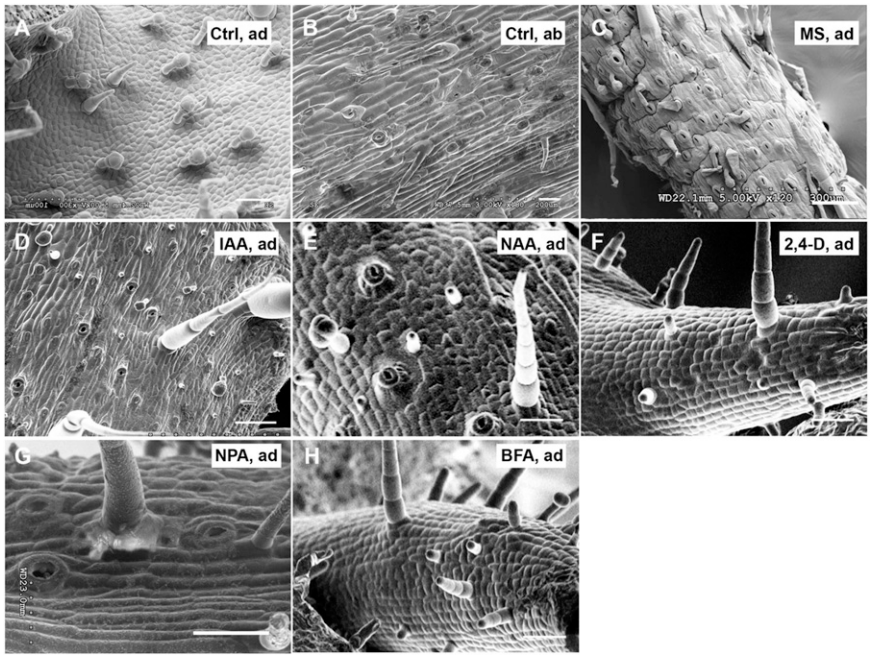

Fig. S6. Epidermis of abaxialized leaf primordia after microapplication of polar auxin transport inhibitors, auxin, or auxin analogs. Control (Ctrl) tomato leaf primordium P_5 adaxial epidermis (*A*) and abaxial epidermis (*B*); leaf primordia adaxial epidermis after microsurgery (MS) incision (*C*); IAA (*D*), NAA (*E*), or 2,4-D (*F*) treatment of the adaxial domain; NPA (*G*) or BFA (*H*) isolation of the primordium. (Scale bars: 50 μm.) ab, abaxial domain; ad, adaxial domain.

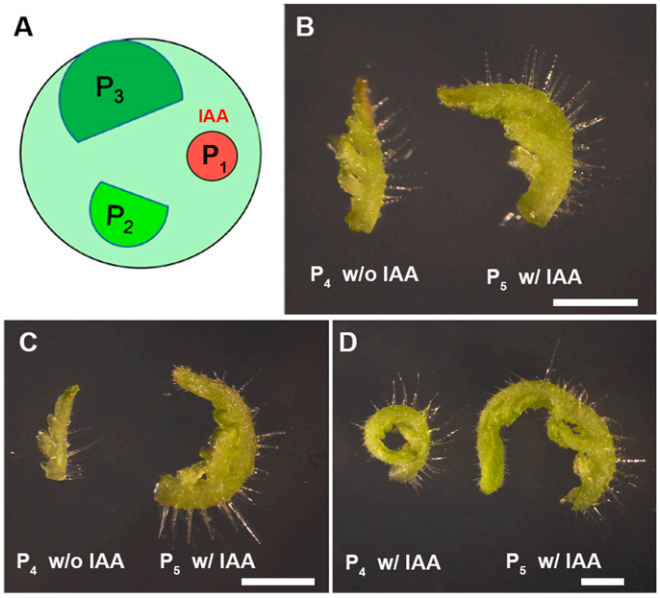

Fig. S7. Applying IAA to an entire emerging P_1 primordium leads to bending toward the shoot apex but not polarity changes. (*A*) Cartoon showing local IAA microapplication (red area) to an entire P_1. (*B–D*) Representative tomato leaves after IAA microapplication as shown in *A* and neighboring leaves without IAA microapplication. Leaves in the image were from the same tomato plant. Leaves were labeled with leaf stage at which photos were taken. (Scale bars: 1 mm.)

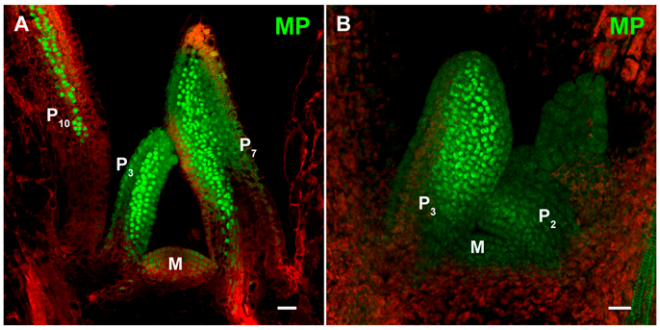

Fig. S8. Expression of MP-GFP (green) in the vegetative shoot apex and leaf primordia. Transverse sections of meristem and primordia showing *pMP::MP-GFP* (green) signals in young leaf primordia are adaxial enriched. *A* is stained by PI (red), and *B* shows chlorophyll autofluorescence in red.

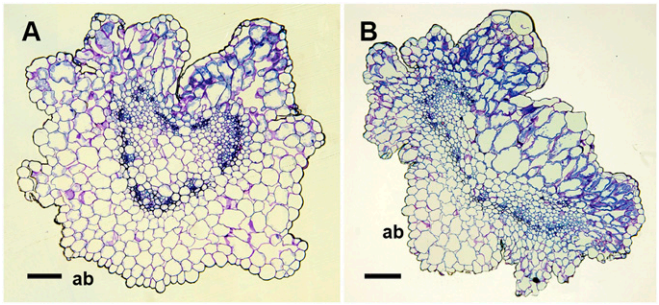

Fig. S9. Leaf abaxialization in *pMP::MP*Δ transgenic plants. Transverse sections through petiole region (*A*) and blade region (*B*) of trumpet-like leaves from *pMP::MP*Δ transgenic plants. (Scale bars: 100 μm.)

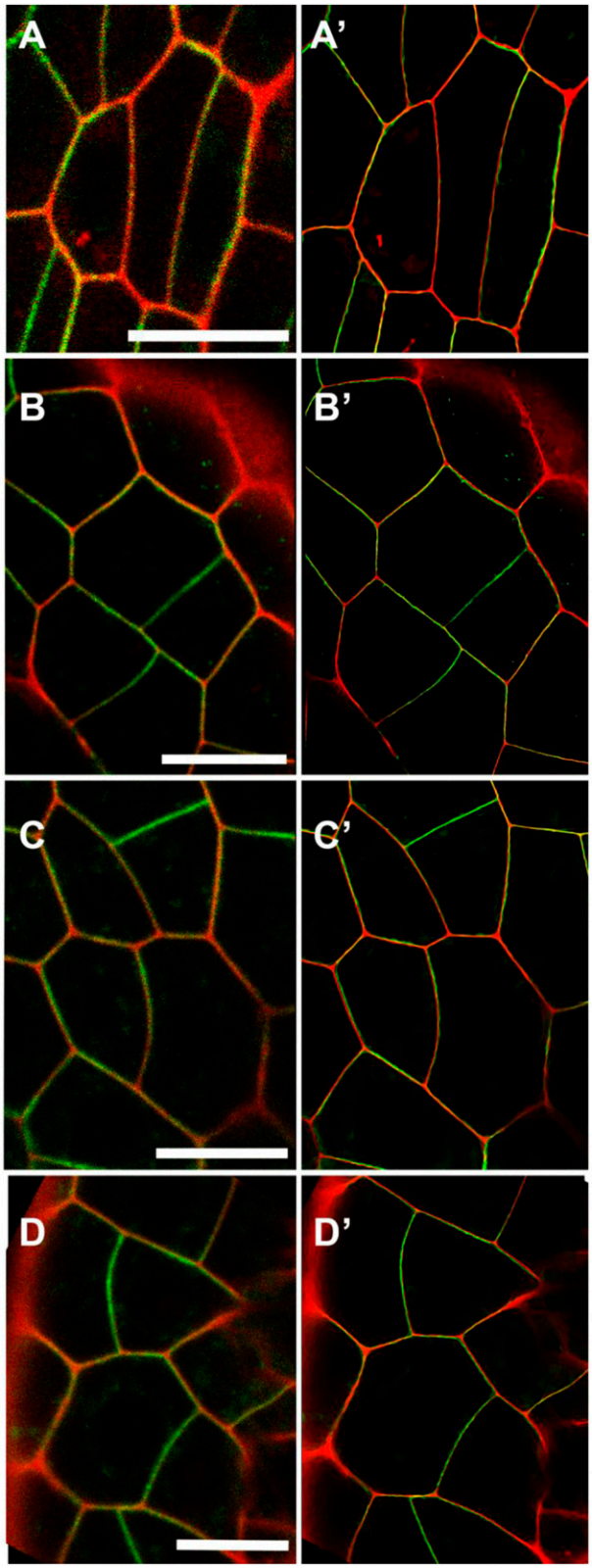

Fig. S10. Comparison of high-resolution AtPIN1-GFP images before and after denoising, contrast enhancement, and morphological erosion. High-resolution images before (*Left*) and after (*Right*) image processing are shown (see *Materials and Methods*). *A* and *B* correspond to the Fig. 3*A Inset*, *C* corresponds to the Fig. 3*D Inset*, and *D* corresponds to the Fig. 3*E Inset*. The cell wall was stained by PI (red), and AtPIN1-GFP is shown in green. (Scale bars, 10 μm.)

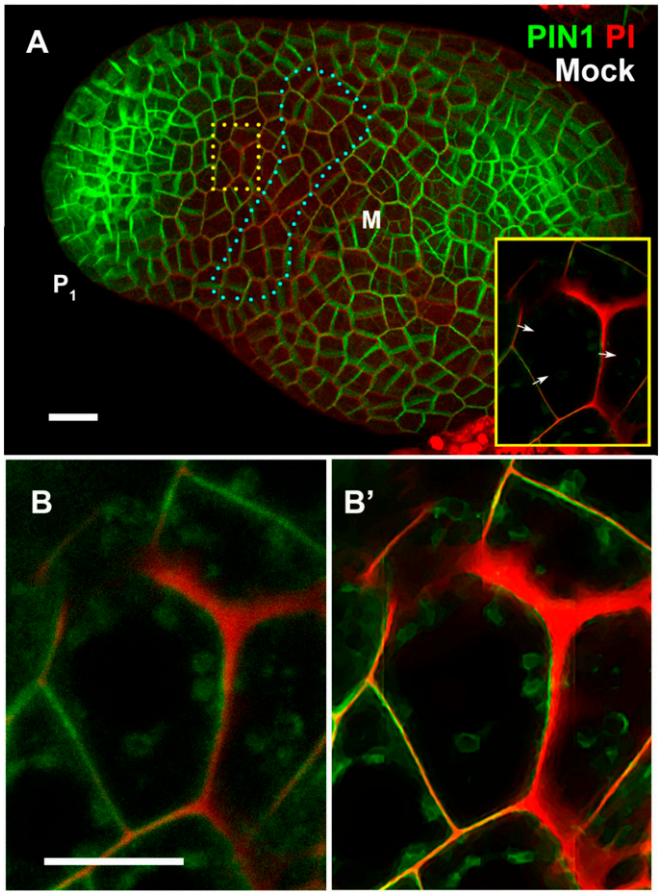

Fig. S11. PIN1 localization in a tomato shoot apex treated with lanolin alone. (*A*) Maximum intensity projections of a tomato *pAtPIN1::AtPIN1-GFP* (green) expressing-meristem stained by PI (red) view from above. The region in the yellow dotted line box was imaged at enhanced resolution and are shown in the yellow box after denoising and contrast enhancement to highlight polar localization of AtPIN1-GFP (the image without denoising and contrast enhancement is shown in *B*). Tomato meristems were treated with lanolin paste alone, with treated area highlighted by a blue dotted line circle. Image was acquired 24 h after treatment. AtPIN1-GFP polarity is shown by white arrows. (*B*) High-resolution images before (*Left*) and after (*Right*) denoising and contrast enhancement are shown. Horizontal flipping was applied to all images to keep a similar orientation as in Fig. 3. (Scale bars: *A*, 20 μm; *B*, 10 μm.)

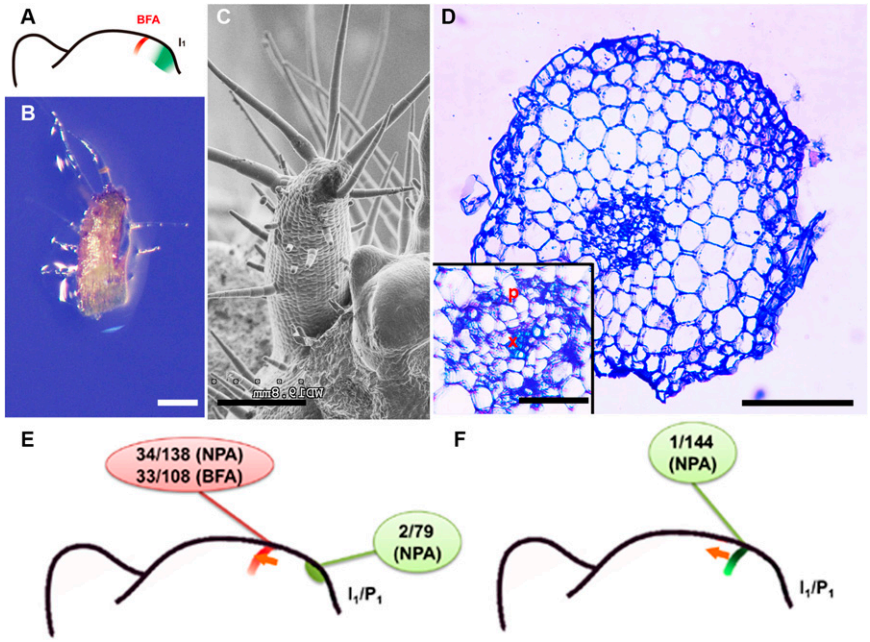

Fig. S12. Microapplication of polar auxin transport inhibitors induces abaxialized radially symmetric leaves. (*A*–*D*) Tomato leaf primordia after local BFA microapplication (*A*), showing early leaf (*B*) and more mature (*C*) primordia with strong defects in adaxial-abaxial polarity, and a transverse section through the midrib and adjacent laminal regions (*D*). (*E*) NPA or BFA treatment between primordium and the SAM leads to high ratios of polarity defects, whereas NPA treatment in a primordium leads to a low ratio of polarity defects. (*F*) NPA treatment at the boundary region of a primordium leads to a low ratio of polarity defects. (Scale bars: 200 μm, except *D Inset*, 50 μm.)

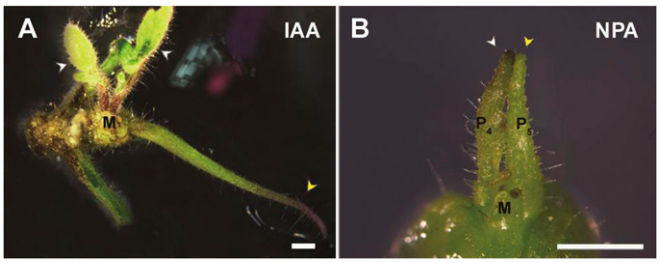

Fig. S13. Microapplication of IAA or NPA affects phyllotaxis. (*A*) A tomato meristem in top view. The adaixal domain of one incipient leaf primordium (yellow arrowhead) was applied with IAA as shown in Fig. S2*A*. Note an apparent reduction in the divergence angle between the next two leaves initiated thereafter (white arrowheads). The light stereomicrograph was taken 9 d after application. (*B*) A tomato meristem in side view. One incipient leaf primordium (yellow arrowhead) was separated from the remainder of the meristem by NPA-containing lanolin paste as shown in Fig. S2*B*. Note an apparent reduction in the divergence angle between the treated leaf and the next leaf initiated thereafter (white arrowhead). The light stereomicrograph was taken 7 d after application. (Scale bars: 1 mm.)

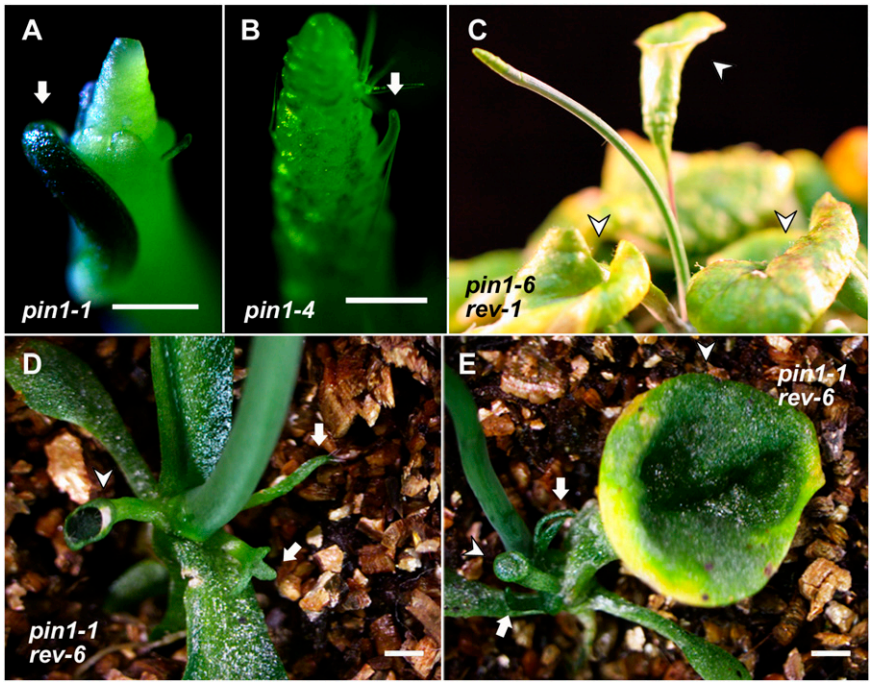

Fig. S14. Adaxial-abaxial polarity phenotypes associated with polar auxin transport defects. Radialized rod-like structures found in *pin1-1* (*A*), *pin1-4* (*B*), and trumpet-like leaves in *pin1-6 rev-1* (*C*) and *pin1-1 rev-6* (*D* and *E*) plants. Arrowheads indicate trumpet-shaped leaves, and arrows indicate rod-shaped leaves. (Scale bars: 1 mm.)

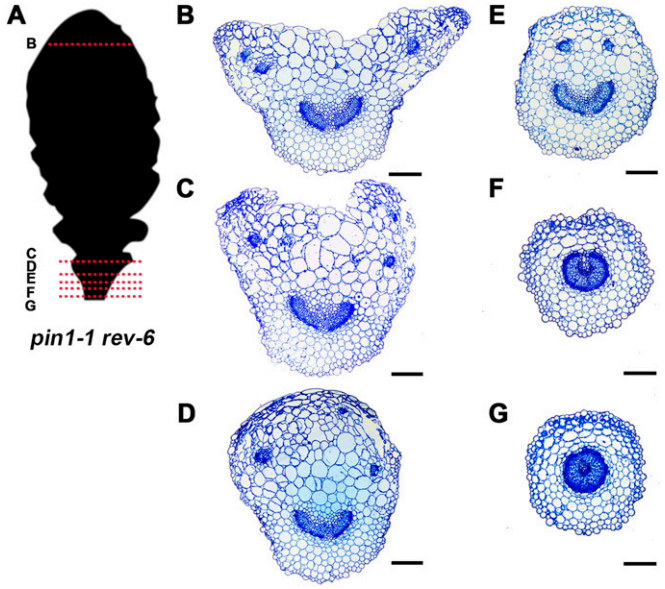

Fig. S15. Adaxial-abaxial polarity phenotypes in normal-shaped *pin1-1 rev-6* leaves. Transverse sections through different regions of a regular-shaped *pin1-1 rev-6* leaf as indicated in *A*. Note regular vascular tissue arrangement in the blade (*B*–*E*) and abaxialized vascular tissue in the petiole (*F* and *G*). (Scale bars: 50 μm.)

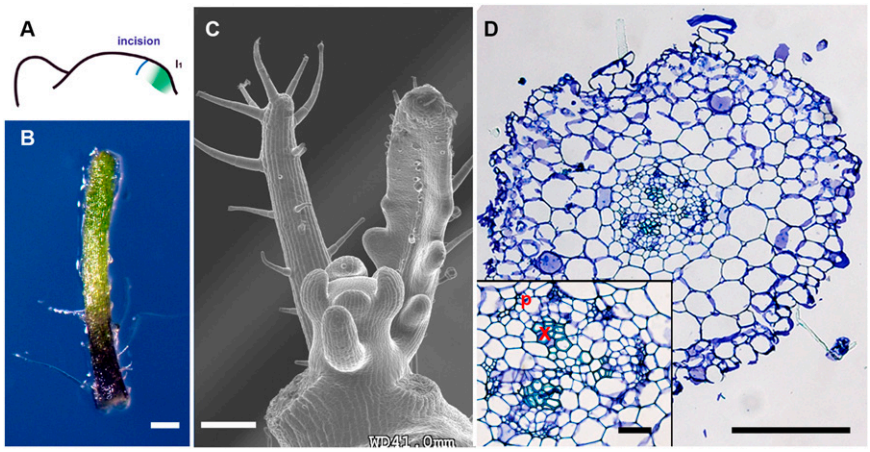

Fig. S16. Microsurgery-induced abaxialized radially symmetric leaves. Tomato leaf primordia after isolation from the meristem, showing the effect of microsurgery on auxin flow (*A*), early leaf (*B*) and more mature (*C*) primordia with strong defects in adaxial-abaxial polarity, and a transverse section through the midrib and adjacent laminal regions (*D*). (Scale bars: 200 μm, except *D Inset*, 50 μm.)

Table S1. Adaxial-abaxial polarity phenotypes associated with polar auxin transport or auxin signaling defects

Genotype	Trumpet-like leaves	Radial rod-like leaves	Total leaf number/ Total plants counted	Percentage of polarity defects, %
Ws	0	0	2,731/100	0
Enkheim	0	0	1,249/48	0
Col-0	0	0	2,593/100	0
*pMP::MP*Δ	64	53	401/30	29
*pAS2::MP*Δ	57	40	387/30	25
pin1-1 (strong)	21	64	326/30	26
pin1-4 (weak)	0	73	540/30	14
pid-6 (null)	0	0	602/30	0
pid-7.2.1.6 (strong)	0	0	595/29	0
rev-1	0	0	681/30	0
rev-6 (in Col-0)	0	0	633/29	0
pin1-1 rev-6	26	41	149/31	45
pin1-1/+ rev-6	0	0	390/30	0
pid-6 rev-6	25	58	621/30	13
pid-6/+ rev-6	0	0	427/26	0
pid-7.2.1.6 rev-1	15	32	727/35	11
pid-7.2.1.6/+ rev-1	0	0	443/20	0